Supporting Information

Chen et al. 10.1073/pnas.1424106112

SI Results

We confirmed the spatial extent and location of each lesion to verify our interpretation of the fMRI findings. Fig. 3*C* shows with postmortem histology a reconstructed lesion (indicated by the black patch), which extended from the dorsal column (targeted white matter tract) to the ventral horn of the left side spinal cord. The coronal slice taken at the dorsal column (indicated by the black line box in Fig. 3*G*) showed clearly the spatial extent of the lesion along the long axis of the spinal cord. On the corresponding MRI image (Fig. 3 *C*, *1*, taken 4 wk after injury) the lesion appeared as a distinct signal void (black hole). The corresponding histological CTB-stained slice (Fig. 3 *C*, *2*) confirmed the location as between the C4 and C5 level and the nature of the lesion. Examination of the CTB dense stains at the entering zone of the digit afferents (see the *Right* image in Fig. 3 *C*, *2*) further confirmed that the lesion was placed in the rostral portion of the left D1 afferent entrance zone in this animal. For each digit, the afferent entrance zone spread ∼2.5 mm along a rostral to dorsal direction along the cord (1). In no animal did the injury extend to the contralateral side of the spinal cord.

SI Discussion

The high spatial resolution (submillimeter) and high contrast-to-noise ratio achievable at high field were central to the success of this study. We demonstrated that using customized coil and appropriate imaging acquisition and analysis techniques, it is possible to achieve high image signal-to-noise ratio, excellent gray–white matter contrast, precise image alignments, and an accurate delineation and sensitive detection of stimuli-evoked fMRI activations and rsFC. High-contrast MTC images permitted better localization of stimulus-evoked fMRI activations to the dorsal and ventral horns. The validity of our fMRI approach is well supported by the postmortem histology (2). One final note is that 3-mm-thick axial image slices acquired in this study approximately sample fMRI responses from one spinal segment in squirrel monkeys (1, 3). Therefore, data acquisition of five 3-mm-thick consecutive axial images allowed the assessment of the functional connectivity change along the cord and showed that the horn–horn connectivity is somatotopically organized.

SI Materials and Methods

Animal Preparation. Five adult (6–8 y old) male squirrel monkeys (*S. sciureus*) were included in this study. Two animals underwent unilateral dorsal column injuries at the high cervical spinal cord level (C4 and C5) after normal prelesion data were collected. During each MRI scan, the monkey was anesthetized with isoflurane (0.5–1.5%) and mechanically ventilated, with head and body stabilized in a magnetic resonance (MR)-compatible frame. Vital signals (cardiac and respiratory cycles, temperature, End Tidal CO_2, and pulse oximetry) were monitored and maintained at appropriate ranges throughout the imaging session. All procedures were performed under a protocol approved by the Institutional Animal Care and Use Committee at Vanderbilt University.

MRI Data Acquisition. MRI scans were performed on an Agilent 9.4T scanner using a saddle-shaped transmit–receive surface coil (2.5 × 3 cm^2 in size) positioned over the animal's neck. Five contiguous axial slices (each 3 mm in thickness), with the third slice positioned over the C5 segment (where the lesion was later targeted in two animals), were acquired in each imaging session. High-resolution (0.25 × 0.25 mm^2 in-plane resolution, 128 × 128 matrix) structural images with MTC [TR (repetition time)/TE (echo time), 220/3.24 ms] were acquired using a Gaussian radio frequency (RF) saturation pulse (flip angle, 820°; pulse width, 12 ms; RF offset, 5,000 Hz). fMRI imaging data were collected with the same five-slice prescription with an in-plane resolution of 0.5 × 0.5 mm^2 (64 × 64 matrix) using a fast gradient echo sequence (flip angle, ∼15°; TE, 6.5 ms; TR, 24 ms; volume acquisition time, 1.54 s).

In Vivo fMRI Data Acquisition. Both stimulus-driven and resting-state fMRI runs contained 300–330 volumes. Multiple runs (four to six) usually were collected for each condition in each animal. Noxious heat stimuli were delivered via a thermal probe positioned over the distal finger pads of D2 and D3, and innocuous tactile stimuli were delivered via a 2-mm-diameter round probe. For each noxious heat stimulation run, 21-s duration blocks of 47.5 °C heat were repeated nine times with a 30-s baseline (32 °C) in between. A 30-s on/off paradigm was used for tactile stimulation, which was a 0.44-mm probe vertical indentation at a 8-Hz rate.

For resting-state fMRI acquisitions, a total of 15 runs were collected from 5 animals in normal (or prelesion) condition, and a total of 10 runs were obtained from subject SM-P at postlesion week 8, 12, and 24 and subject SM-G at postlesion week 2, 3, 7, 10, and 15. After injury, both animals exhibited behavioral deficits in a food reaching and retrieval task for about 6 wk. Locations of the spinal nerve afferent bundles and their spatial relationships with the spinal cord were used as landmarks to align axial imaging plans across imaging sessions of the same animal and across animals.

fMRI Data Analysis.

Preprocessing. The fMRI images were initially preprocessed with slice time correction followed by 2D rigid body motion correction based on maximization of mutual information with an initial reference scan. A standard matlab routine (imregister2) was used to estimate three motion parameters (two translation and one rotation) for each slice, and all of the derived translation and rotation parameters were within 1 mm. The fMRI images were next up-sampled to 0.25 × 0.25 mm (from 0.5 × 0.5 mm) resolution for the second step of preprocessing. Two "nuisance" signals were derived from a principal components analysis of the time courses of voxels in muscle and cerebrospinal fluid, respectively. The first three to five signal components that accounted for at least 70% of the cumulative signal variance in each region were used, along with the motion correction parameters, as regressors in a general linear model to reduce their contributions to the fMRI signal. The resting-state fMRI signals were then band pass filtered (cutoff frequencies, 0.01 and 0.1 Hz) using a Chebyshev type II filter. The preprocessed fMRI images were manually aligned to the corresponding MTC structural images. This manual alignment step was performed for each slice within each run and for all runs in each subject.

ROI-based analysis. An ROI-based correlation analysis was conducted to assess the inter-ROI functional connectivity using customized software in SPM5/8. This approach was preferred to data-driven methods such as independent component analysis because the results are more robust and the selections of the ROIs could be made based on hypotheses derived from our stimulus-driven studies and previous fMRI studies in humans. Each ROI was manually selected on a slice-by-slice basis according to the aligned high-resolution gray–white matter axial MTC images. Fig. 1 *A*–*C* showed the sagittal, coronal, and axial MTC images of the spinal cord. The gray matter appeared to be brighter than the white matter on these images. The clear butterfly shape of gray matter allowed a more accurate selection of ROI seed voxels within the

gray and white matter. Four ROI seeds were identified at each central portion of the dorsal and ventral horns of the spinal cord, and a control ROI seed was selected within the white matter region. The location of the control seed was randomized across runs and animals. Each ROI typically contained two to three voxels. In after lesion conditions, data from slice 3 (where the lesion was placed) were excluded in the quantification.

Statistical analysis. The correlations between the mean fMRI signal time courses of each paired ROI seeds were calculated. The average values of the correlation coefficients associated with each ROI were taken for future statistical analysis at the group level. Correlation strengths among horn (ventral and dorsal) and control ROIs were compared in a pair-wise manner within each slice (intraslice ROIs) and across slices (interslice ROIs). The statistical significance of the differences between the correlation coefficient values of ROI pairs was determined using a non-parametric Mann–Whitney Wilcoxon test. A result of $P < 0.05$ was interpreted to be statistically significant. Statistical analysis was conducted only at the animal group level. We excluded outliers, which were defined as data points that exceeded 98% confidence interval ($|z| > 2.236$), in the group quantification. A statistical threshold of a z score, which was an inter- or intraslice ROI correlation coefficient of $r > 0.35$, was selected to protect against type I errors (false positive correlation).

Spinal Cord Lesion. Two animals were anesthetized with a high isoflurane level (2–3%) for the lesion surgery under aseptic conditions. The dorsal column was sectioned on the right side with a fine pair of surgical scissors at cervical level C4 and C5. The dura were then replaced with Gelfilm and covered with Gelfoam, and the skin was sutured. Monkeys were recovered and carefully monitored after each procedure. Further details of the surgical procedures can be found in our previous publications (3, 4). Animal behaviors on a food reaching and retrieval task were qualitatively assessed before and after the lesion. Both animals exhibited apparent impairments on this task within the first 6 wk after lesion.

1. Florence SL, Wall JT, Kaas JH (1991) Central projections from the skin of the hand in squirrel monkeys. *J Comp Neurol* 311(4):563–578.
2. Wang F, et al. (2014) Multiparametric MRI reveals dynamic changes in molecular signatures of injured spinal cord in monkeys. *Magn Reson Med*, 10.1002/mrm.25488.
3. Qi HX, Chen LM, Kaas JH (2011) Reorganization of somatosensory cortical areas 3b and 1 after unilateral section of dorsal columns of the spinal cord in squirrel monkeys. *J Neurosci* 31(38):13662–13675.
4. Chen LM, Qi HX, Kaas JH (2012) Dynamic reorganization of digit representations in somatosensory cortex of nonhuman primates after spinal cord injury. *J Neurosci* 32(42): 14649–14663.

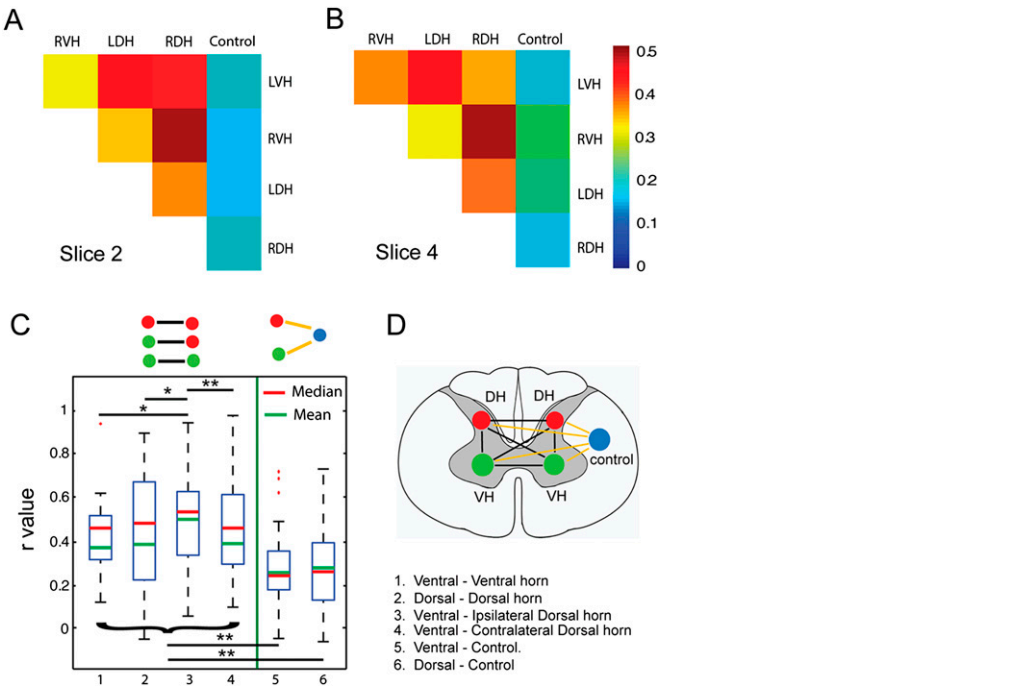

Fig. S1. Differential correlation strengths among intraslice ROIs in normal animals. (*A* and *B*) 2D correlation matrix plots of the mean correlation coefficients among intraslice ROI pairs in two separate image slices (*A*, slice 2; *B*, slice 4), respectively. The color of the squares indicated the strength of the correlation (see color scale bar for *r* values). (*C*) Whisker box plot shows the distribution of correlation coefficients across all ROI pairs. The upper and lower bounds of the box indicate the upper and lower quartile of the data. Red stars indicate the outlier. The red and green lines inside the blue box indicate the mean and median values, respectively. Green line separates the two ROI pairs groups: horn–horn pairs (columns *1–4*) and horn–control pairs (columns *5* and *6*). Intraslice ROI measures from all five image slices were included in the quantification for each animal. Fifteen sets of data from five animals were included in the group analyses. Error bars are SD. $*P < 0.01$; $**P < 0.001$. (*D*) A schematic diagram shows the possible pair-wise correlation analysis (indicated by color lines) among all five ROIs within one single axial image slice: two ventral horns, two dorsal horns, and one white matter control.

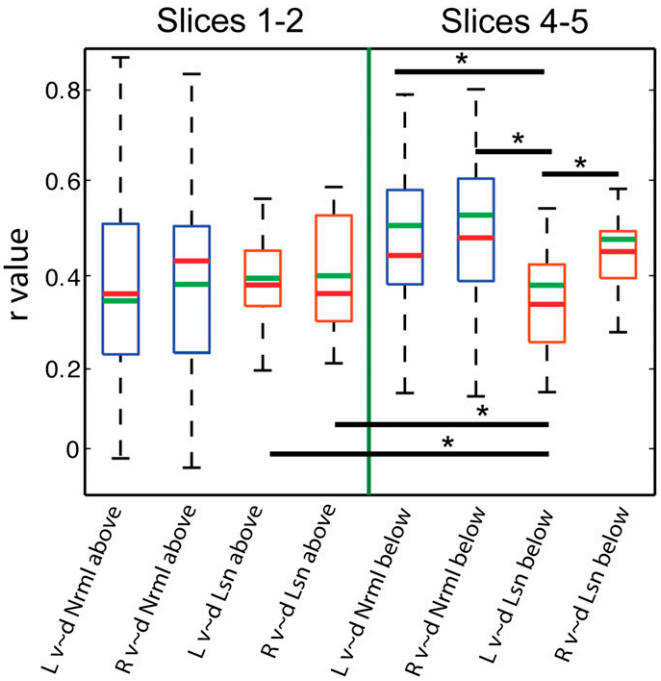

Fig. S2. Group comparison of intraslice ventral–dorsal horn connectivity in rostral (slices 1 and 2) versus caudal slices (slices 4 and 5) of normal and lesion animals. Whisker box plots of the mean and distribution of correlation coefficients of intraslice ventral–dorsal pairs (v–d) in rostral (slices 1 and 2, above lesion slices in lesioned animals) and dorsal (slices 4 and 5, below lesion slices in lesioned animals) slices in normal (Nrml) and lesioned (Lsn) animals. Correlation values obtained from two slices (1 and 2 or 4 and 5) were pooled together in the quantification. Slice 3 in both normal and lesioned animals (lesion slice) were excluded in the analysis. $*P < 0.05$ (no parametric Mann-Whitney test).